ADVANCED FUNCTIONAL MATERIALS
www.afm-journal.de

Quinoidal Molecules as a New Class of Ambipolar Semiconductor Originating from Amphoteric Redox Behavior

Hansu Hwang, Dongyoon Khim, Jin-Mun Yun, Eunhwan Jung, Soo-Young Jang, Yun Hee Jang, Yong-Young Noh, and Dong-Yu Kim**

The two small molecules, quinoidal bithiophene (QBT) and quinoidal biselenophene (QBS), are designed based on a quinoid structure, and synthesized via a facile synthetic route. These quinoidal molecules have a reduced band gap and an amphoteric redox behavior, which is caused by an extended delocalization. Due to such properties, organic field-effect transistors based on QBT and QBS have shown balanced ambipolar characteristics. After thermal annealing, the performances of the devices are enhanced by an increase in crystallinity. The field-effect hole and electron mobilities are measured to be 0.031 $cm^2 V^{-1} s^{-1}$ and 0.005 $cm^2 V^{-1} s^{-1}$ for QBT, and 0.055 $cm^2 V^{-1} s^{-1}$ and 0.021 $cm^2 V^{-1} s^{-1}$ for QBS, respectively. In addition, we investigate the effect of chalcogen atoms (S and Se) on the molecular properties. The optical, electrochemical properties and electronic structures are mainly dominated by the quinoidal structure, whereas molecular properties are scarcely affected by either type of chalcogen atom. The main effect of the chalcogen atoms is ascribed to the difference of crystallinity. Due to a strong intermolecular interaction of the selenophene, QBS exhibits a higher degree of crystallinity, which leads to an enhancement of both hole and electron mobilities. Consequently, these types of quinoidal molecules are found to be promising for use as ambipolar semiconductors.

1. Introduction

Great efforts toward the design and synthesis of organic semiconducting materials have resulted in impressive progress in the field of organic field-effect transistors (OFETs), with performances exceeding that of amorphous silicon.[1] Numerous *p*-channel, *n*-channel, and ambipolar organic semiconductors have been successfully developed in both small molecular and polymeric semiconductors through the exploration of diverse π-conjugated building blocks such as acences, oligothiophenes, fused aromatics, etc.[2] Recently, ambipolar OFETs have attracted much attention in both scientific and industrial areas, because of their potential applications in complementary metal-oxide semiconductor (CMOS)-like logic circuits and organic light emitting transistors (OLETs).[3] Furthermore, CMOS-like inverters based on ambipolar materials can be simply fabricated without additional patterning of individual FETs.[4] Generally, ambipolarity in single components can be easily achieved from low band gap polymers due to the well-matched energy levels with work function of metal electrodes.[5] On the other hand, organic small molecular semiconductors have rarely exhibited ambipolar properties because of the difficulty in obtaining a low band gap and suitable energy levels, which causes poor charge injection.[6] Nevertheless, the appropriate selection and fine tuning of the chemical structures of small molecules in some cases could provide sufficiently low injection barriers for holes and electrons, which leads to ambipolar properties.[7]

Among various conjugated molecular building blocks, quinoidal molecules have attracted considerable interest as a new class of semiconducting materials for organic electronics.[8] Compared with conventional aromatic organic semiconductors, several features of quinoidal molecules are of interest. First, these molecules have a highly planar structure that is favorable for π–π stacking, leading to an efficient charge transport in the solid state.[9] Second, quinoidal structures dramatically lower the band gap compared with common aromatic structures.[10] The aromaticity of the molecules is reduced with an increasing quinoidal character, which allows the delocalization of confined π-electrons in the aromatic ring, resulting in a reduction in band gap.[11] Last, a significant feature of the quinoidal structure is its amphoteric redox behavior, which refers to simultaneous oxidation and reduction in the same component.[12] In general, oxidation [reduction] is correlated with the injection of holes [electrons] into the highest occupied molecular orbital (HOMO) level [the lowest unoccupied molecular orbital (LUMO) level], respectively. Therefore, the features of quinoidal molecules make them good candidates as both *p*-type and *n*-type semiconductors when they are properly polarized. In other

H. Hwang, Dr. D. Khim, E. Jung, S.-Y. Jang, Prof. Y. H. Jang, Prof. D.-Y. Kim
School of Materials Science and Engineering
Gwangju Institute of Science and Technology (GIST)
261 Cheomdan-gwagiro, Buk-gu, Gwangju 500–712, Republic of Korea
E-mail: kimdy@gist.ac.kr
Dr. J.-M. Yun
Radiation Research Division for Industry and Environment
Korea Atomic Energy Research Institute (KAERI)
29 Geumgu-gil, Jeongeup-si, Jeollabuk-do 580–185, Republic of Korea
Dr. D. Khim, Prof. Y.-Y. Noh
Department of Energy and Materials Engineering
Dongguk University
26 Pil-dong, 3-ga, Jung-gu, Seoul 100–715, Republic of Korea
E-mail: yynoh@dongguk.edu

DOI: 10.1002/adfm.201402758

words, quinoidal molecules are most likely promising ambipolar materials, which are capable of transporting both hole and electron carriers within a single component under suitable conditions and device configurations.

Until now, the most efficient strategy to obtain quinoidal molecules has been the incorporation of dicyanomethylene (DCM) groups at both termini.[13] Most semiconductors containing DCM groups have shown *n*-channel FET behaviors due to the strong electron affinity of the DCM group.[14] Even though they have a low band gap, most of them were expected to show *n*-type behaviors, since the strong electron affinity of the DCM group creates a large injection barrier between the HOMO level and the work function of electrodes. However, ambipolar properties of quinoidal compounds have been reported in some cases with a modulation of energy levels via chemical modification.[15] Their ambipolar properties most likely originate from the amphoteric redox behavior and low band gap of quinoidal character.[16] On the other hand, such DCM substituted quinoidal molecules usually show poor solubility in common organic solvents especially when the chain is extended.[17] To overcome this problem, many research groups have tried to modify the central core unit by solubilizing bulky building blocks such as a cyclopentane ring,[15a,18] or to substitute the terminal group with an alkylated ester or a carbonyl instead of the cyano group.[19] These strategies can make the quinoidal molecules more soluble in organic solvents, which can facilitate device fabrication via a solution process. However, steric bulkiness of the solubilizing group hampers molecular ordering in the solid state, resulting in a decrease in device performance.

Here, we suggest unusual quinoidal molecules without a DCM group, quinoidal bithiophene (QBT) and quinoidal biselenophene (QBS), as semiconductors for ambipolar OFETs. A synthetic route for quinoidal bithiophene (QBT) has been reported by Tormos et al.[20] After starting from the alkylation of isatin to the N-position, only sulfuric acid treatment to the alkyl-substituted isatin with a thiophene gave quinoidal bithiophene. This approach provides two major advantages: first, a facile synthetic method compared with DCM-substituted molecules due to the absence of complicated steps such as bromination or Pd-based reaction, and second is the ease of solubility control by just a simple variation in the solubilizing group at the N-position of the isatin molecule. In this research, we carefully chose a dodecyl solubilizing group in order to increase solubility as well as induce molecular ordering in the solid state. Recently, several groups reported that the replacement of thiophene with selenophene in polymers or small molecules showed enhanced field-effect mobilities due to a strong intermolecular interaction between selenium atoms.[21] Selenophene containing quinoidal molecules showed similar results.[22] For this purpose, we synthesized and characterized QBS, as well as QBT, in accordance with previously established methods in the literature.[20] As expected, both molecules showed a significant reduction in band gap and also an amphoteric redox behavior, which gives rise to ambipolar properties. In addition, we report the first application of these types of quinoidal molecules to organic field-effect transistors, and observed well-balanced excellent ambipolar properties.

2. Results and Discussion

2.1. Synthesis and Thermal Characterization

The synthesis of the quinoidal small molecules (QBT and QBS) was carried out according to procedures established in the literature,[20] as shown in **Scheme 1**. A long linear dodecyl alkyl chain was introduced at the N-position of the starting material (Isatin, 1) in order to accomplish solubility with common organic solvents such as THF, chloroform and chlorobenzene. Additionally, the reaction of N-dodecylisatin with thiophene or selenophene promoted by sulfuric acid afforded a dark blue QBT and QBS. The final products were characterized by ^{1}H-NMR, MALDI-TOF, and elemental analysis. As expected, all these compounds showed good solubility at room temperature in common organic solvents such as chloroform (18 mg mL^{-1}) and chlorobenzene (≈12 mg mL^{-1}). This high solubility facilitates the fabrication of OFET devices based on spin coating. Due to the double-bond linkage between chalcogenophenes, there were six configurational isomers in the final products, as shown in Figure S2 (Supporting Information). It was difficult to separate the mixed isomers, and also complicated to analyze the quantitative ratio of each isomer due to intricately overlapped NMR spectra (Figure S1, Supporting Information). Note that there is no obvious evidence that coexistent isomers decrease the device performance in quinoidal molecule-based OFETs. Despite co-existent isomers, previously reported quinoidal molecules showed an electron mobility of up to 0.016 cm^2 V^{-1} s^{-1}.[15a] Additionally, another example was also reported that isomers of mixed molecules showed a mobility similar to that of isomer-free molecules.[19a]

Thermogravimetric analysis (TGA) showed thermal decomposition temperatures of 270 and 325 °C for QBT and QBS, respectively (Figure S3, Supporting Information). It is well known that the thermal stability of molecules containing selenophene is higher than that of thiophene analogues.[23] Strong intermolecular interaction between the Se···Se atom probably lead to the higher thermal stability of the QBS containing selenophene. From the differential scanning calorimetry (DSC) measurement, as shown in Figure S4 (Supporting Information), clear endothermic transition upon heating and exothermic transition upon cooling were observed for both molecules. Interestingly, there are two endothermic peaks for QBS at 201 and 223 °C. It can be speculated that two endothermic peaks of QBS come from different thermal behavior of mixed

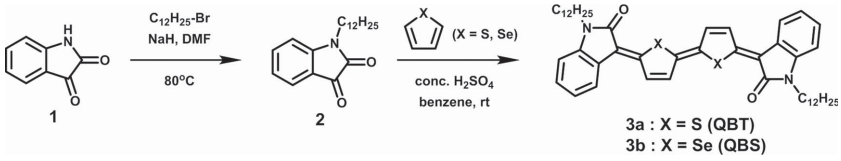

Scheme 1. Synthetic route of the quinoidal bithiophene (QBT) and quinoidal biselenophene (QBS).

Adv. Funct. Mater. **2015**,
DOI: 10.1002/adfm.201402758

isomers; since evidences for mesophase formation could not be found (see the Supporting Information).

2.2. Optical and Electrochemical Properties

The UV–vis absorption spectra of both QBT and QBS were measured as thin films and in chloroform solutions in order to understand optical properties. As shown in **Figure 1**a and 1b, the absorption onset of both compounds was similarly located at long wavelengths of approximately 775 and 825 nm in solution and in thin films, respectively. The corresponding optical band gaps were approximately 1.6 and 1.5 eV, respectively. Even though only two chalcogenophene units were incorporated into both molecules, a significant reduction in band gap was observed, which is originated from an increase in delocalized π-electrons of quinoidal structures. The optical properties of both molecules showed similar behavior regardless of chalcogenophene, particularly in the case of absorption spectra in solution.

In addition, both quinoidal molecules exhibited broader absorptions from 350 to 830 nm and well-defined vibronic peaks in the thin films compared to those in solution. This might indicate that these quinoidal molecules have strong intermolecular interactions in the solid state. Interestingly, both QBT and QBS showed blue-shifted absorption maxima (≈50–60 nm) with complex band splitting in the solid state compared to that in solution. Such complex band structures were attributed to complex molecular organization. Even though the origin of such blue shifts and complex band structures was not clarified, certain H-type aggregation is a likely cause.[24] When the molecules whose transitional moments follow the long molecular axis form parallel-stacked dimers (H-aggregation), the transitional coupling splits into two levels of excited state. The upper transition is allowed, along with the summation of transition moments, while the transition moments of the lower transition can cancel each other out, resulting in a forbidden transition.[25] Similarly, common quinoidal molecules containing DCM groups also show similar optical properties.[14b,19]

The intensity of the vibronic shoulder was enhanced by increasing the annealing temperature of the films, as shown in Figure S5 (Supporting Information), which would imply the increases in intermolecular interactions upon annealing.[26] When the vibronic peaks of the QBS thin film were compared with those of QBT, more well-defined vibronic splitting was observed at 628 and 683 nm. This vibronic splitting implies a more highly ordered structure of QBS in the solid state,[27] which demonstrates that a high degree of crystallinity is expected for the QBS film.

To evaluate the electrochemical properties of both molecules, cyclic voltammetry as thin film was measured in 0.1 M Bu_4NClO_4 in acetonitrile solution. The cyclic voltammograms of both molecules and the corresponding energy levels were presented in **Figure 2**. As expected, the oxidation as well as the reduction potentials of two molecules were obtained, which is amphoteric redox behavior. Similar redox behaviors were observed in thienoquinoidals when the quinoidal core is extended.[9,12,15c,16] This amphoteric redox behavior can provide ambipolar property in OFET devices. The HOMO and LUMO energy levels of each compound were calculated from the onset of the each potential wave. Corresponding HOMO and LUMO levels of QBT are −5.25 and −3.76 eV, respectively; and those of QBS are −5.33 and −3.73 eV, respectively. All the optoelectronic parameters such as optical band gap, electrochemical band gap, absorption maximum, HOMO level, and LUMO level were summarized in **Table 1**. Both molecules showed almost similar molecular properties, which means that molecular properties are largely affected by quinoidal character in this type of

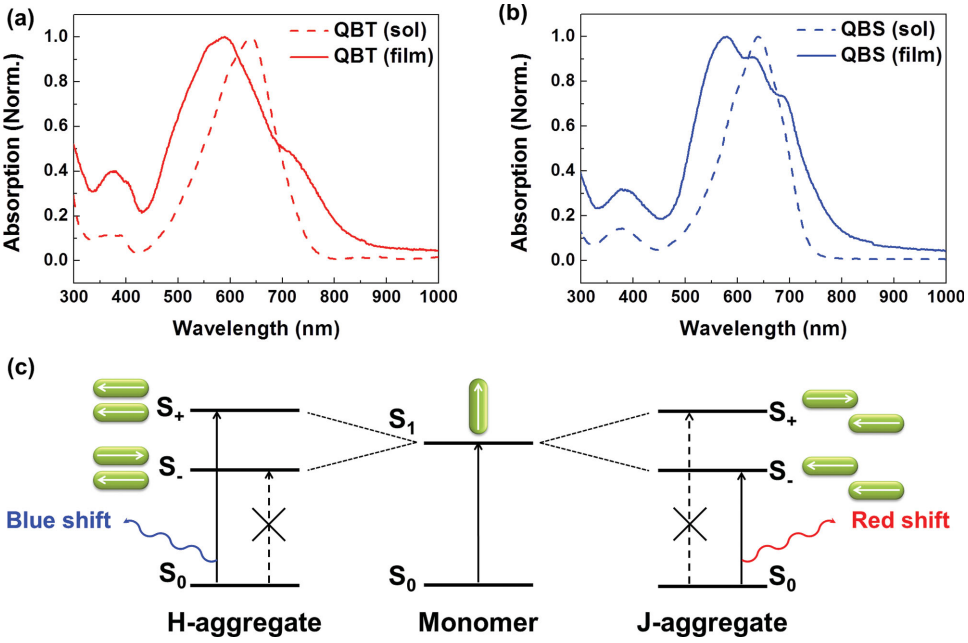

Figure 1. UV–vis absorption spectra of a) QBT and b) QBS in chloroform solution and thin film. c) Schematic diagram of electronic transitions in H- and J-aggregated molecules.

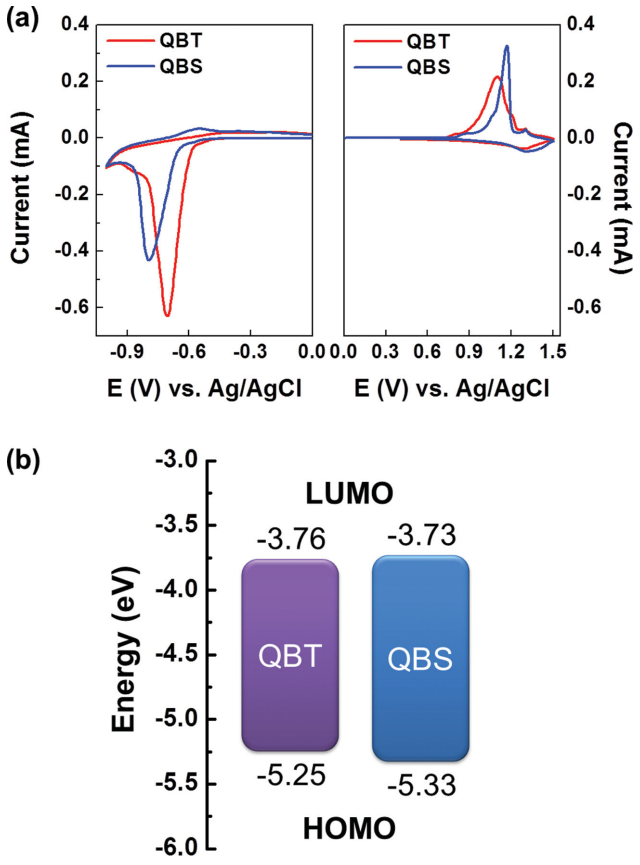

Figure 2. a) Cyclic voltammograms of QBT and QBS thin films in 0.1 M Bu_4NClO_4 solution in ACN with scan rate of 50 mV s^{-1}. b) Energy level diagrams of QBT and QBS.

molecules. The optical and electrochemical results demonstrate that quinoid structure gives rise to impressive features which are low band gap and amphoteric redox behavior. Taking into account those features, the ambipolarity of both QBT and QBS can be expected.

2.3. Molecular Geometry and Electronic Structure Calculation

In order to further estimate the electronic structure and molecular geometry, density functional theory (DFT) calculations were carried out on structures with the methyl groups replaced at the N-positions for simple calculations. We selected two *trans*-like configurational structures between central units, iso 1 and iso 2, among coexistent six isomers for the calculations, as shown in **Figure 3**a. These isomers were selected because the *trans*-form between adjacent thiophene rings is energetically more stable than the *cis*-form.[28] In addition, we assumed that the molecular geometry and the electronic structures of all isomers would be similar. To assure that both molecules are independent of the isomeric structures, the electronic structures of not only *trans*-isomers but also one *cis*-isomer (iso 6) were calculated by DFT (Figures S6 and S7, Supporting Information). The optimized geometries and calculated frontier molecular orbitals of the two isomers of QBT and QBS are shown in Figure 3b. All isomers of both quinoidal molecules were completely planar owing to a double-bond linkage (dihedral angle between each ring is 0°). This highly planar structure could be beneficial for charge transport.

Accordingly, all isomers of both molecules showed a well distributed electron density for both HOMO and LUMO along the entire backbone. Regardless of isomer structure and the type of introduced chalcogenophenes (thiophene or selenophene), the electron densities of HOMO and LUMO displayed almost identical distributions, particularly along the quinoidal backbone. The well distributed HOMO and LUMO of these two molecules manifested a significant delocalization of the quinoidal structure, which agreed with the amphoteric redox behavior shown in the above CV results. These results also indicate that such quinoidal molecules are potential candidates for ambipolar materials. The electron densities of the HOMO and LUMO showed no differences with respect to the isomeric structures (*trans*- and *cis*-isomers), similar to the geometric results. In accordance with the speculation, molecular geometry and electronic structure are determined by quinoid structure, and not the isomeric configuration.

The calculated HOMO and LUMO were −5.17 and −3.27 eV, respectively, for iso 1 of QBT, and −5.25 and −3.29 eV, respectively, for iso 2 of QBT. In the case of QBS, the calculated HOMO and LUMO were −5.22 and −3.30 eV, respectively, for iso 1, and −5.30 and −3.31 eV, respectively, for iso 2. The HOMO and LUMO levels of each isomer were not exactly identical; however, each value was similar and agreed with CV results. The slight difference between the calculated LUMO and estimated LUMO from CV was attributed to different conditions. The calculation was performed on a single molecule in gas phase, while CV was measured as a thin film in the solution.

In addition, the computed vertical excitation and oscillator strength (*f*) were investigated by using time-dependent (TD) DFT calculations. The calculated absorption properties of iso 1 as a single molecule for both QBT and QBS are shown in Figure S8 (Supporting Information). The main electronic transition with strong oscillator strength was located at 652 nm for QBT and 644 nm for QBS (see the Supporting Information). Such oscillator strengths of both molecules were in good agreement with the experimental absorption maxima in solution (640 nm for QBT and QBS). Because molecules in dilute

Table 1. Optical and electrochemical properties of QBT and QBS.

	E_g^{opt}, film [eV]	E_g^{opt}, sol [eV]	λ_{max}, film [nm]	λ_{max}, sol [nm]	HOMO [eV]	LUMO [eV]	E_g^{CV} [eV]
QBT	1.50	1.60	590	640	−5.25	−3.76	1.49
QBS	1.53	1.63	580	640	−5.33	−3.73	1.60

DOI: 10.1002/adfm.201402758

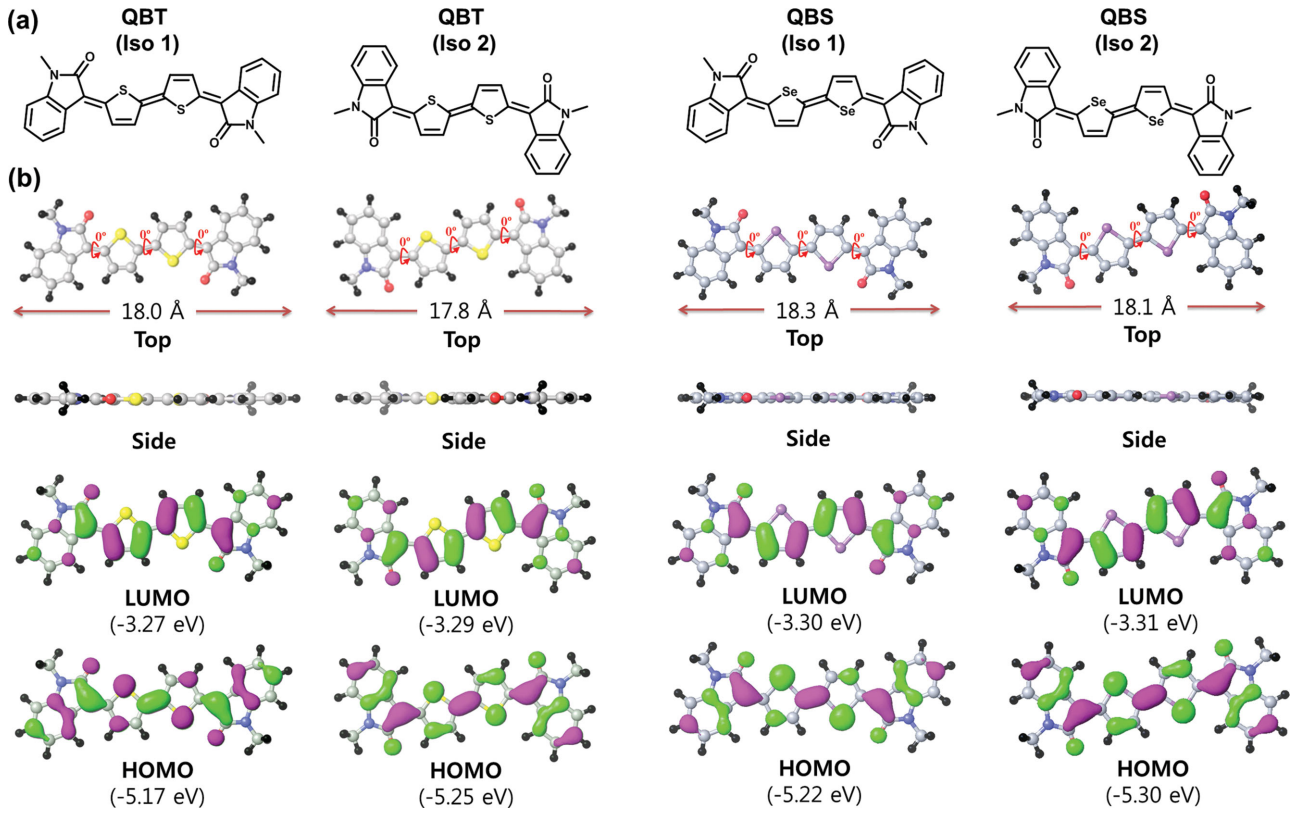

Figure 3. a) Selected *trans*-based chemical structures for calculations between possible isomers of QBT and QBS. b) Optimized molecular geometries and their molecular orbital diagrams from DFT calculation.

solutions are regarded as a single isolated molecule, calculated absorption from TD-DFT correlates well with absorption in solution.

2.4. Characterization of Field-Effect Transistor Devices

To investigate the feasibility of an ambipolar semiconductor for these types of quinoidal molecules, organic field-effect transistors with top-gate/bottom-contact (TG/BC) configurations were fabricated by spin coating. The details of the transistor fabrication process are described in the Experimental Section. The measured field-effect mobility (μ_{FET}) and threshold voltage (V_{th}) are summarized in **Table 2**, and the output and transfer characteristics of the annealed QBT and QBS films at 170 °C are shown in **Figure 4**. The output characteristics showed a linear regime at low voltage and a current saturation regime at high voltage; furthermore, a small degree of

Table 2. Summary of OFET parameters of QBT- and QBS-based devices.

	Ann. temp.	Hole			Electron		
		μ_h [cm^2 V^{-1} s^{-1}]	$V_{th,h}$ [a)] [V]	I_{On}/I_{Off} [b)]	μ_e [cm^2 V^{-1} s^{-1}]	$V_{th,e}$ [V]	I_{On}/I_{Off}
QBT	as-spun	4.1×10^{-3} [c)]	-36.8 ± 1.1	10^{3-4}	5.8×10^{-5}	46.3 ± 3.9	10^{3-4}
	(Average)	3.5×10^{-3} ($\pm 6.0 \times 10^{-3}$) [d)]			3.2×10^{-5} ($\pm 2.6 \times 10^{-5}$)		
	170 °C	3.1×10^{-2}	-39.1 ± 5.3	10^{7-8}	5.0×10^{-3}	49.4 ± 7.8	10^{5-6}
	(Average)	2.9×10^{-2} ($\pm 2.0 \times 10^{-3}$)			4.6×10^{-3} ($\pm 5.2 \times 10^{-4}$)		
QBS	as-spun	1.3×10^{-3}	-43.7 ± 2.3	10^{4-5}	4.6×10^{-4}	37.2 ± 5.1	10^{3-4}
	(Average)	1.1×10^{-3} ($\pm 1.7 \times 10^{-4}$)			4.3×10^{-4} ($\pm 3.0 \times 10^{-5}$)		
	170 °C	5.5×10^{-2}	-41.1 ± 3.1	10^{6-7}	2.1×10^{-2}	35.9 ± 3.1	10^{4-5}
	(Average)	5.3×10^{-2} ($\pm 2.0 \times 10^{-3}$)			1.8×10^{-2} ($\pm 3.0 \times 10^{-3}$)		

[a)]Average threshold voltage measured from 8 to 10 devices; [b)]Current on:off ratios (I_{On}/I_{Off}) are obtained at $V_{DS} = \pm 20$ V; [c)]Maximum field-effect mobilities; [d)]Average field-effect mobilities were measured for 8 to 10 devices.

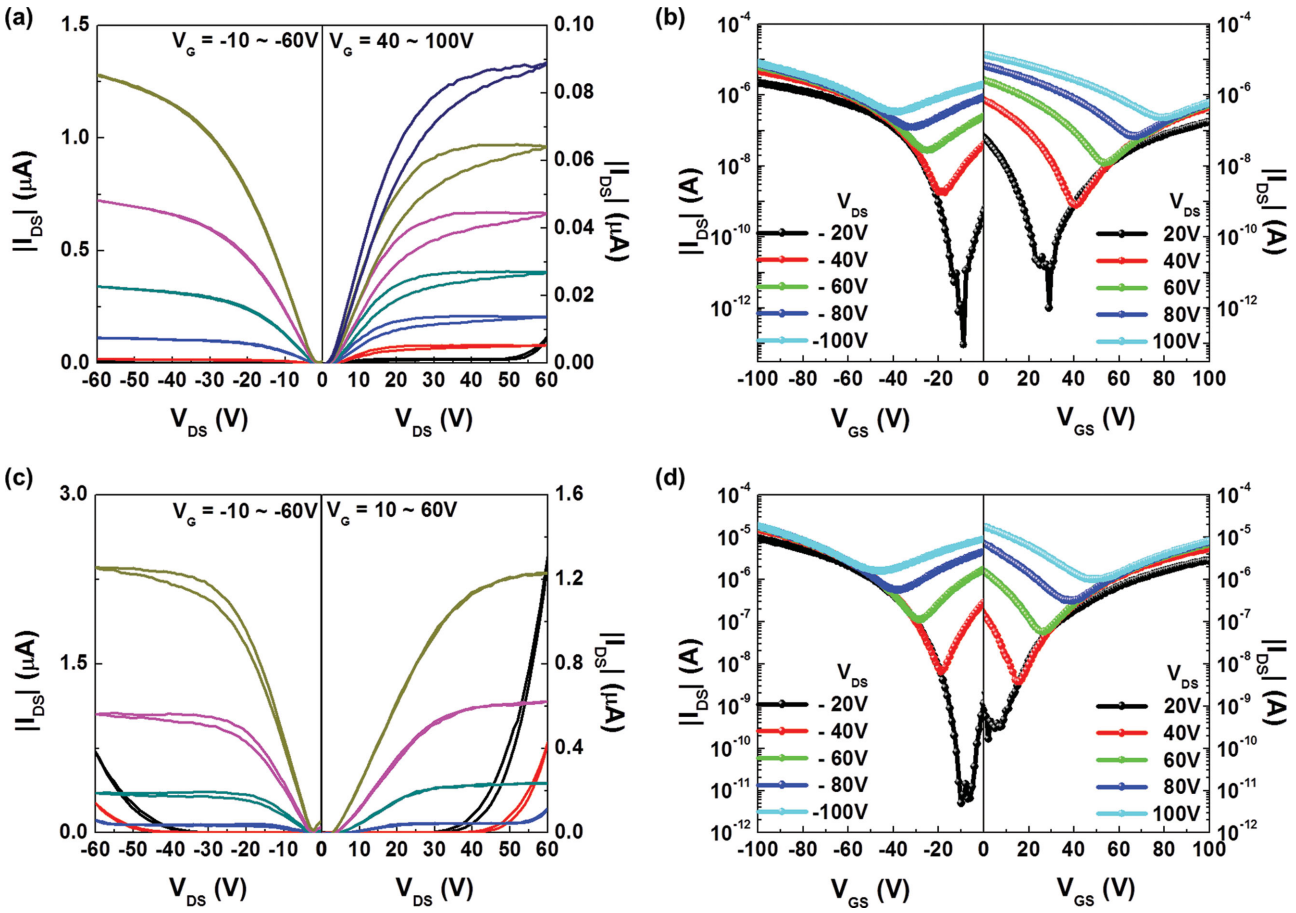

Figure 4. Output and transfer characteristics of OFETs based on a,b) QBT and c,d) QBS films annealed at 170 °C.

hysteresis and contact resistance was also observed. Despite slight contact resistance, the output characteristics showed desirable linear and saturation regimes with drain-voltage dependence. When gold (Au) was used for the bottom-contact electrodes with π-conjugated molecules, the effective work function was reduced to −4.5 eV compared with that of cleaned bulk Au (−5.1 eV) due to a "push-back" effect on the metal/organic interfaces.[29] Consequently, the hole and electron charge injection barriers were approximately ≈ 0.8 eV, which was enough for an efficient charge injection of both carriers (The HOMO was approximately −5.3 eV and the LUMO was approximately −3.7 eV).

Additionally, in good accordance with the low band gap and amphoteric redox properties of the quinoid structures discussed above, the OFETs based on both QBT and QBS showed the V-shaped transfer characteristics of typical ambipolar transistors as illustrated in Figure 4b,d. The hole and electron mobilities were extracted from the saturation regime of the transfer curve, as shown in Figure S9 (Supporting Information). The as-spun films of the two molecules exhibited relatively low hole and electron mobilities of 4.1×10^{-3} and 5.8×10^{-5} cm^2 V^{-1} s^{-1} for QBT, and 1.3×10^{-3} and 4.6×10^{-5} cm^2 V^{-1} s^{-1} for QBS, respectively. However, the both hole and electron mobilities of the two molecules were gradually enhanced as annealing temperature was increased up to 170 °C, and the maximum hole and electron mobilities at this temperature were 0.031 and 0.005 cm^2 V^{-1} s^{-1} for QBT, and 0.055 and 0.021 cm^2 V^{-1} s^{-1} for QBS, respectively. Such enhanced mobilities upon thermal annealing were considered to be due to an improved film crystallinity, which will be discussed later. In spite of the coexistent six isomers, their mobilities were comparable or slightly higher than common DCM containing molecules comprised of similar chain lengths such as dimers[22] or even trimers.[15a] The average hole and electron mobilities for QBT and QBS are shown in **Figure 5** as a function of the annealing temperature. When the film was annealed at temperatures as high as 200 °C, FET mobilities started to decline. Such an annealing temperature (200 °C) was close to the melting point observed in the DSC measurement for both molecules, which demonstrated that the crystalline phase had collapsed at approximately 200 °C, leading to a reduction of mobility.

When comparing the differences in mobility between thiophene and selenophene derivatives, the device based on QBS showed a more enhanced hole and electron mobility than that of QBT. As mentioned above in the CV and DFT results, the two molecules showed almost identical energy levels and electron densities of the HOMO and LUMO frontier molecular orbitals. Therefore, their mobility difference might have arisen from their differences in crystallinity rather than from electronic structure. Commonly, molecules containing selenophene

DOI: 10.1002/adfm.201402758

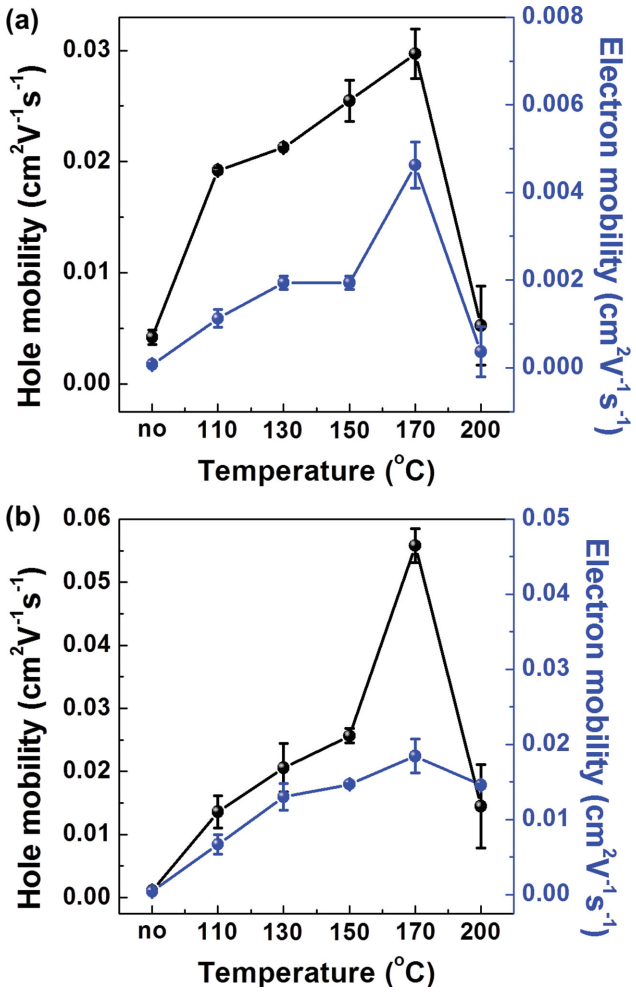

Figure 5. Average field-effect hole and electron mobilities depending on annealing temperatures. a) QBT and b) QBS.

exhibit a strong intermolecular interaction and a higher crystallinity compared to thiophene derivatives, resulting in enhanced charge transport properties.[21,22] Selenophene derivatives have a strong intermolecular interaction due to an increase in electron donating and in the polarizable properties of selenophene compared to that of thiophene, which originate from the larger atomic radius of Se.[23] Hence, the OFETs based on QBS showed improved hole and electron mobilities compared to QBT.

2.5. Crystallinity and Thin Film Morphology

To elucidate the enhanced mobility upon thermal annealing, the crystallinity and the surface morphology were investigated using X-ray diffraction (XRD) and atomic force microscopy (AFM) depending on differences in the annealing temperature. In order to explore the crystal structure, the growth of single crystals of QBT and QBS was attempted by using physical vapor and solution-based methods. The single crystals of QBT and QBS, however, could not be grown by either method. First, we attempted sublimation of both molecules under high vacuum (≈10^{-8} Torr);[30] however, they did not sublime, but degraded

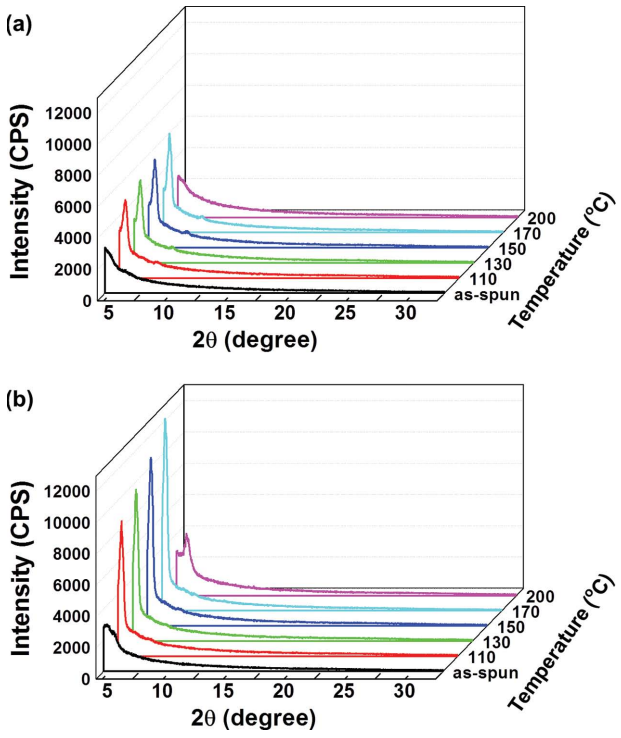

Figure 6. Out-of-plane X-ray diffraction patterns of spin-coated films of a) QBT and b) QBS at different annealing temperatures.

when high power was applied. This might be due to the high molecular weights and strong intermolecular interactions of QBT and QBS. Second, we tried solution-based methods such as recrystallization and slow evaporation with various solvents.[13b,31] We also could not obtain any crystals using these solution methods, and only precipitation was obtained. Instead of clarifying the single crystal structure, molecular dimensions obtained from DFT calculations could be useful for simple estimation of crystallinity.[30a,32] In this study, QBT and QBS molecular sizes were defined by DFT calculations to speculate the orientation and crystallinity of the molecules in thin films measured from out-of-plane XRD. The thin films of both molecules were prepared by spin coating a chlorobenzene solution onto the Si/SiO_2, followed by annealing at different temperatures. **Figure 6** shows the out-of-plane XRD diffraction patterns of QBT and QBS. The as-spun films of both molecules showed no clear diffraction pattern, whereas obvious diffraction peaks were observed and the intensity of each peak was steadily amplified as the annealing temperature increased up to 170 °C. The increasing intensity of the XRD patterns is consistent with increases in device performance, even with a decrease in performance at 200 °C. The intensity of the films annealed at 200 °C (the approximate melting point) was dissipated or weakened, which indicates a diminished crystallinity and results in a decrease in mobility. The crystallinity changes measured by XRD are also in agreement with the changes of the vibronic shoulder in UV–vis absorption upon annealing, as shown in Figure S5 (Supporting Information).

QBT diffraction peaks were observed at 2.49° corresponding to a *d*-spacing of 35.48 Å. For QBS, the peaks appeared at 2.45° with a *d*-spacing of 36.08 Å, and the molecular end-to-end

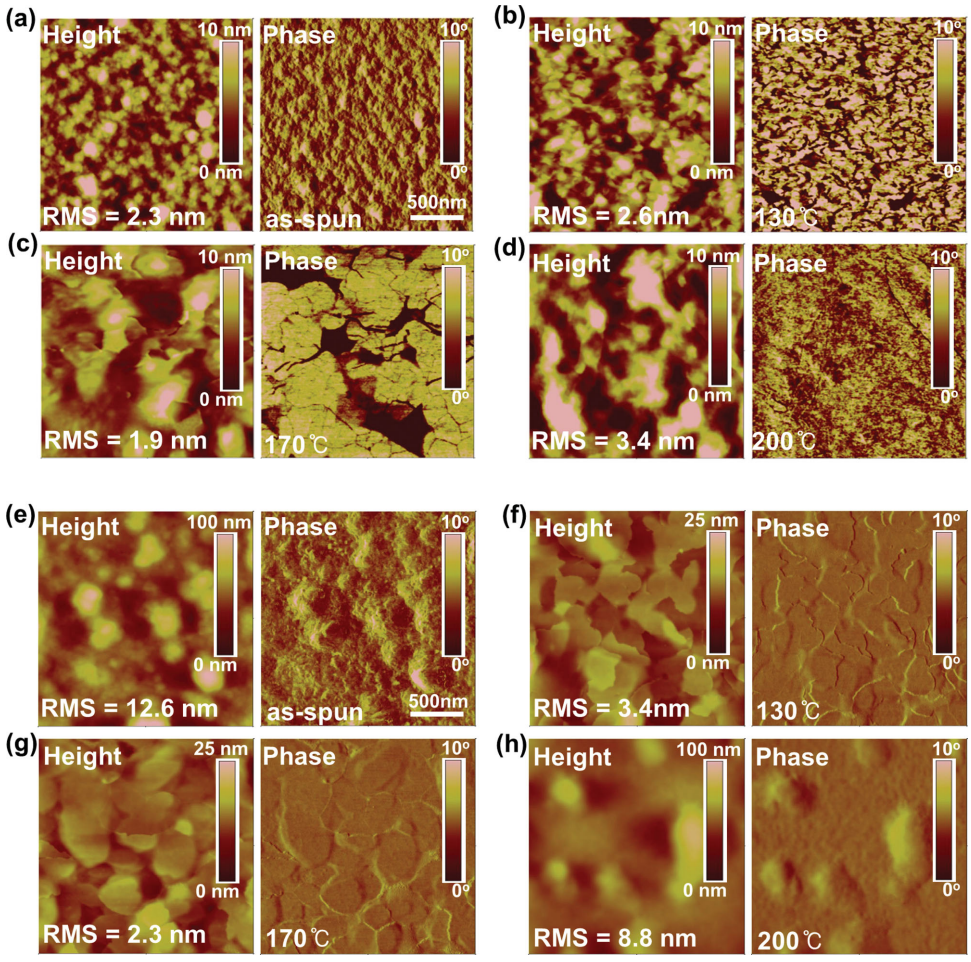

Figure 7. AFM height and phase images of spin-coated films of a–d) QBT and e–h) QBS at different annealing temperatures.

length was calculated during the DFT investigation. As shown in Figure 4, the molecular lengths of the isomeric structures were 17.8 Å for iso 1 and 18.0 Å for iso 2 in the case of QBT, and 18.1 Å for iso 1 and 18.3 Å for iso 2, repectively, in the case of QBS. The *d*-spacing estimated from the XRD pattern correlated with twice the molecular length. Therefore, it would be reasonable to speculate on the end-to-end packing of both molecules with respect to the substrate. In addition, the diffraction peaks of QBS film exhibited a stronger intensity compared to that of QBT, which meant that QBS had a higher degree of crystallinity than that of QBT. This was most likely due to the strong intermolecular interaction of the selenophene. Taking into account strong crystallinity, the device based on QBS showed a more enhanced mobility, as previously mentioned.

The morphologies of QBT and QBS were measured by tapping-mode AFM as thin film prepared on a glass substrate at different annealing temperatures. The AFM height and phase images of both molecules are shown in **Figure 7**. Each as-spun film showed an aggregated granular surface with many grain boundaries, as shown in Figure 7a,e for QBT and QBS, respectively. Upon thermal annealing up to 170 °C, the grain sizes of both QBT and QBS films were continuously increased and interconnected, and there was a decrease in the root-mean-square (RMS) roughness. As shown in Figure 7c,g, the thin films annealed at 170 °C finally exhibited a terraced morphology with a low roughness and a decreased grain boundary, which led to an improvement in device performance. These morphological changes might have been affected by the growth of the crystal domain. As mentioned above, and shown in Figure 6, the crystallinity of annealed films was decreased at high temperature around the melting point. As a result, the grains were excessively aggregated and the RMS roughness was again increased at 200 °C, which caused a decrease in the mobility of OFET devices. Consequently, the device performance upon thermal annealing was mainly affected by the changes in crystallinity and surface morphology, as shown by the XRD and AFM measurements.

2.6. Characterization of Complementary Inverter

Based on the optimization of annealing conditions, we also fabricated complementary-like inverters that consisted of two identical ambipolar QBS OFETs. A solution-processed ambipolar QBS was easily deposited via spin-coating without additional sophisticated patterning processes for each of the *p*- and *n*-channel regions. In order to match the current level of *n*- and *p*-channel regions of OFETs, the W/L ratios

Adv. Funct. Mater. **2015**,
DOI: 10.1002/adfm.201402758

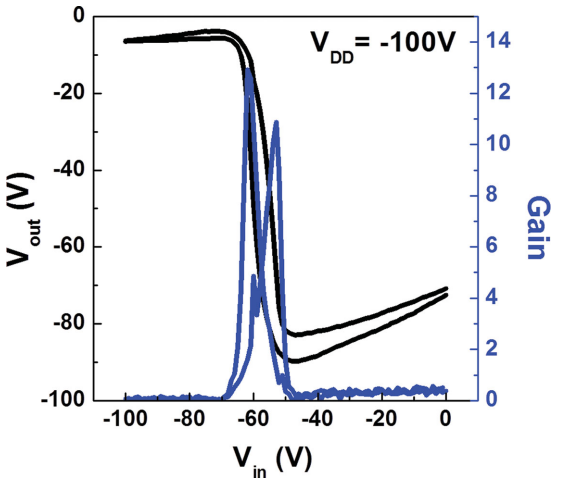

Figure 8. Voltage transfer characteristics and voltage gain of CMOS-like inverter based on QBS film.

for the *n*- and *p*-channel region OFETs were adjusted to 5:1 ($L_{p,n}$ = 20 μm, W_n = 5 mm, W_p = 1 mm). Details of the fabrication process are included in the Experimental Section. The voltage transfer characteristics (VTCs) showed an ideal symmetry with a switching voltage nearly half of the power supply (V_{DD}) as shown in **Figure 8**, and corresponding voltage gain exhibited relatively high gain (≈13) at a supplied voltage (V_{DD}) of –100 V.

3. Conclusions

In conclusion, we successfully synthesized quinoidal molecules, QBT and QBS, for use as ambipolar organic semiconductors. The quinoidal characteristics led to unusual features compared with common aromatic molecules. Both QBT and QBS showed a significantly low band gap and broad absorption despite a short conjugation length; interestingly, they exhibited a blue shift in the absorption maxima in the solid state due to the formation of H-aggregates. Electrochemical studies verified the amphoteric redox behavior of the two quinoidal molecules. Regardless of the kinds of chalcogen atoms, both molecules showed similar molecular properties. In addition, very well-distributed electron densities for the HOMO and LUMO of both molecules are also identical. Consequently, all these properties arose from the quinoid structure; and this gave rise to ambipolar properties when applied to OFETs. Solution-processed TG/BC OFETs based on QBT and QBS thin films predictably showed ambipolar characteristics. After optimization via thermal annealing, enhanced hole and electron mobilities with increased crystallinity and well-balanced ambipolar characteristics were observed. Additionally, the selenophene-containing QBS showed increased crystallinity and enhanced mobility compared to the thiophene analogue (QBT), because selenophene exhibits a stronger intermolecular interaction due to larger and more polarizable Se atoms. Finally, we fabricated a complementary-like inverter based on balanced ambipolar QBS film, and the inverter exhibited a high voltage gain of ≈13 with a switching voltage that approximated $V_{DD}/2$. Therefore, our results demonstrate that these types of quinoidal molecules are a promising class of ambipolar materials.

4. Experimental Section

Materials and Characterization: All starting materials were purchased from Sigma-Aldrich Chemical Co., Tokyo Chemical Industry Co., or Alfa Aesar Co., and were used without further purification. ^{1}H-NMR spectra were measured using a JEOL ECX-400P, 400 MHz in $CDCl_3$. Mass data were obtained via gas chromatography mass spectrometry (GC-MS) (Shimadzu, GCMS-QP2010), and MALDI-TOF Mass spectrometer (AXIMA-CFR, Shimadzu). Elemental analysis was performed on a Flash1112, Flash2000 (CE instrument). Thermogravimetric analysis (PerkinElmer, TGA 4000) and differential scanning calorimetry (PerkinElmer, DSC 4000) were conducted at a heating rate of 10 °C min^{-1} under a nitrogen atmosphere. The UV–vis spectrometry was conducted using a Perkin Elmer Lambada 750. Cyclic voltammetry was recorded on an Eco Chemie Autolab PGSTAT 30 in an acetonitrile solution with 0.1 M tetrabutylammonium perchlorate (Bu_4NClO_4) as the supporting electrolyte, indium tin oxide (ITO) as the working electrode, a Pt wire as the counter electrode, and a Ag/AgCl electrode as the reference electrode at a scan rate of 50 mV s^{-1}. X-ray diffraction (XRD) was measured using a PAnalytical X'Pert PRO Multi Purpose Diffractometer with Cu K radiation. AFM data were measured using tapping-mode atomic force microscopy (Nanoscope III, Veeco Instrument, Inc) at the Korea Basic Science Institute.

*Synthesis of N-Dodecylisatin(**2**)*: Isatin (3 g, 20.39 mmol) was added to a solution of sodium hydride (0.979 g, 40.8 mmol) in anhydrous DMF (60 mL). After stirring for 30 min, 1-bromododecane was added, and the reaction mixture was refluxed overnight. The reaction mixture was cooled to room temperature. The organic layer was extracted with dichloromethane and dried over anhydrous magnesium sulphate ($MgSO_4$). The crude product was purified by column chromatography with dichloromethane and recrystallized from hexane to afford **2** as an orange crystal (3.8 g, 60%). ^{1}H NMR (400 MHz, $CDCl_3$): δ (ppm) 7.6 (*d*, *J* = 7.32 Hz, 1H) 7.58 (*t*, *J* = 7.10 Hz, 1H) 7.11 (*t*, *J* = 7.55 Hz, 1H) 6.89 (*d*, *J* = 8.01, 1H) 3.71 (*t*, *J* = 7.33 Hz, 2H) 1.70 (quin, *J* = 14.48, 7.30 Hz, 2H) 1.41–1.25 (*m*, 18H), 0.88 (*t*, *J* = 6.75, 3H). MS (EI, m/z): $[M]^+$ calcd for $C_{20}H_{29}NO_2$, 315.22; found, 315.20.

*Synthesis of Quinoidal Bithiophene (**3a**)*: Concentrated sulfuric acid (0.1 mL) was added dropwise to a rapidly stirred solution of N-dodecylisatin (643.5 mg, 2.04 mmol) and thiophene (343.3 mg, 4.08 mmol) in benzene (15 mL). After the reaction mixture was stirred for 3h at room temperature, water (50 mL) was added and the product was extracted with chloroform. The organic layer was dried over anhydrous magnesium sulphate ($MgSO_4$). After removal of the solvent under reduced pressure, the crude product was purified twice by column chromatography (chloroform:hexane = 9:1) and precipitated with a cosolvent of chloroform and methanol to afford **3a** as a dark blue solid (324 mg, 41%). MS (MALDI-TOF, m/z): $[M+H]^+$ calcd for $C_{48}H_{62}N_2O_2S_2$, 762.43; found, 763.8. Anal. calcd for $C_{48}H_{62}N_2O_2S_2$: C, 75.55; H, 8.19; N, 3.67; O, 4.19; S, 8.40%; found: C, 74.83; H, 8.18; N, 3.61; O, 4.79; S, 8.39%.

*Synthesis of Quinoidal Biselenophene (**3b**)*: **3b** was prepared according to the procedure for the synthesis of compound **3a** in a 21% (189 mg) yield. MS (MALDI-TOF, m/z): $[M]^+$ calcd for $C_{48}H_{62}N_2O_2S_2$, 858.3; found, 856.3. Anal. calcd for $C_{48}H_{62}N_2O_2S_2$: C, 67.28; H, 7.29; N, 3.27; O, 3.73%; found: C, 67.22; H, 7.26; N, 3.20; O, 3.76%.

OFET Device Fabrication and Characterization: OFET devices were fabricated in the TG/BC configuration. Corning Eagle 2000 glass was used as the substrate with patterned Au/Ni (15/3 nm) source and drain electrodes using conventional lift-off photolithography. The patterned channel width/length was 1.0 mm/20 μm. For cleaning, the substrates were ultrasonicated first in acetone then again in isopropanol, and were exposed to UV/O_3 for 20 min. The semiconductors, QBT and QBS, were dissolved in anhydrous chlorobenzene at a concentration

of 15 mg mL^{-1}, and were spin-coated onto the substrates in a N_2-purged glove box. The solutions were filtered with a 0.45 μm polytetrafluoroethylene (PTFE) syringe filter before spin-coating. The spin-coated films were thermally annealed at 110, 130, 150, 170, and 200 °C for 20 min in a N_2-purged glove box. For the polymer dielectric layers, CYTOP (Asahi Glass) was spin-coated at 2000 rpm for 60 s (≈500 nm). Top gate transistors were finally completed by the deposition of aluminum gate electrodes via thermal evaporation using a metal shadow mask. The electrical characteristics were measured using a Keithley 4200-SCS under a N_2 atmosphere. The field-effect mobility and V_{th} were calculated at the saturation region using gradual channel approximation equations

$$I_{DS} = (W / 2L)\mu C_i(V_G - V_{th})^2 \quad (1)$$

where L is the channel length, W is the channel width, C_i is the capacitance per unit area of the gate dielectric layer, and V_{Th} is the threshold voltage.

Complementary Inverter Fabrication: The substrates with electrical contacts (Au/Ni) of the inverters were prepared by the same process used above. The semiconducting layer of QBS was spin-coated and annealed at 170 °C for 20 min. The remaining processes followed the same procedure as the OFET fabrication.

Quantum Chemical Calculation: The geometries of both QBT and QBS were fully optimized in the gas phase. All the geometry optimization in the ground state was carried out at the B3LYP/6–311G(d,p) level of DFT using the Jaguar v6.5 software.[33] All optimized geometries were confirmed to be the minimum-energy structures using a normal-mode analysis. The HOMO energy levels (E_{HOMO}) of both molecules were taken from the eigenvalues of the Kohn–Sham equation. At the optimized geometry of both molecules, the singlet–singlet electronic transition energies were calculated using the time-dependent DFT (TD-DFT) at the same level of B3LYP/6–311G(d,p) to estimate the HOMO–LUMO energy gaps (E_g) and the LUMO energy levels [$E_{LUMO} = E_{HOMO} + E_g$]. The Gaussian09 program was employed for TD-DFT calculations.[34]

Supporting Information

Supporting Information is available from the Wiley Online Library or from the author.

Acknowledgements

This work was supported by a National Research Foundation of Korea (NRF) grant funded by the Korea Government (MSIP) (Grant Nos. 2013–059210 and 2013R1A1A3012254), and by the Bio Imaging Research Center at GIST, the Center for Advanced Soft Electronics funded by the Ministry of Science, ICT, and Future Planning as a Global Frontier Project (2013M3A6A5073183). The facilities used for the calculations were supported by KISTI via the Grand Challenge Program (KSC-2012-C3–26) and the PLSI Program. We thank the Korea Basic Science Institute (KBSI) for AFM measurements.

Received: August 12, 2014
Revised: November 25, 2014
Published online:

[1] a) J. Mei, Y. Diao, A. L. Appleton, L. Fang, Z. Bao, *J. Am. Chem. Soc.* **2013**, *135*, 6724; b) Y. Yuan, G. Giri, A. L. Ayzner, A. P. Zoombelt, S. C. B. Mannsfeld, J. Chen, D. Nordlund, M. F. Toney, J. Huang, Z. Bao, *Nat. Commun.* **2014**, *5*, 3005; c) H.-R. Tseng, H. Phan, C. Luo, M. Wang, L. A. Perez, S. N. Patel, L. Ying, E. J. Kramer, T.-Q. Nguyen, G. C. Bazan, A. J. Heeger, *Adv. Mater.* **2014**, *26*, 2993.

[2] a) S. Allard, M. Forster, B. Souharce, H. Thiem, U. Scherf, *Angew. Chem., Int. Ed.* **2008**, *47*, 4070; b) H. Dong, C. Wang, W. Hu, *Chem. Commun.* **2010**, *46*, 5211; c) X Guo, R. P. Oritz, Y. Zheng, Y. Hu, Y.-Y. Noh, K.-J. Baeg, A. Facchetti, T. J. Marks, *J. Am. Chem. Soc.* **2011**, *133*, 1405; d) H. Dong, X. Fu, J. Liu, Z. Wang, W. Hu, *Adv. Mater.* **2013**, *25*, 6158.

[3] a) E. J. Meijer, D. M. De Leeuw, S. Setayesh, E. Van Veenendaal, B.-H. Huisman, P. W. M. Blom, J. C. Hummelen, U. Scherf, T. M. Klapwijk, *Nat. Mater.* **2003**, *2*, 678; b) L. Bürgi, M. Turbiez, R. Pfeiffer, F. Bienewald, H.-J. Kirner, C. Winnewisser, *Adv. Mater.* **2008**, *20*, 2217; c) K.-J. Baeg, J. Kim, D. Khim, M. Caironi, D.-Y. Kim, I.-K. You, J. R. Quinn, A. Facchetti, Y.-Y. Noh, *ACS Appl. Mater. Interfaces* **2011**, *3*, 3205; d) K.-J. Baeg, D. Khim, S.-W. Jung, M. Kang, I.-K. You, D.-Y. Kim, A. Facchetti, Y.-Y. Noh, *Adv. Mater.* **2012**, *24*, 5433; e) S. Z. Bisri, C. Piliego, J. Gao, M. A. Loi, *Adv. Mater.* **2014**, *26*, 1176.

[4] a) T. D. Anthopoulos, S. Setayesh, E. Smits, M. Cölle, E. Cantatore, B. de Boer, P. W. M. Blom, D. M. de Leeuw, *Adv. Mater.* **2006**, *18*, 1900; b) D. Khim, H. Han, K.-J. Baeg, J. Kim, S.-W. Kwak, D.-Y. Kim, Y.-Y. Noh, *Adv. Mater.* **2013**, *25*, 4302.

[5] a) J. Zaumseil, H. Sirringhaus, *Chem. Rev.* **2007**, *107*, 1296; b) Z. Chen, H. Lemke, S. Albert Seifried, M. Caironi, M. M. Nielsen, M. Heeney, W. Zhang, I. McCulloch, H. Sirringhaus, *Adv. Mater.* **2010**, *22*, 2371; c) J. Kim, K.-J. Baeg, D. Khim, D. T. James, J.-S. Kim, B. Lim, J.-M. Yun, H.-G. Jeong, P. S. K. Amegadze, Y.-Y. Noh, *Chem. Mater.* **2013**, *25*, 1572; d) A. Luzio, D. Fazzi, D. Natali, E. Giussani, K.-J. Baeg, Z. Chen, Y.-Y. Noh, A. Facchetti, M. Caironi, *Adv.Funct. Mater.* **2014**, *24*, 1151.

[6] G. Zhang, P. Li, L. Tang, J. Ma, X. Wang, H. Lu, B. Kang, K. Cho, L. Qiu, *Chem. Commun.* **2014**, *50*, 3180.

[7] a) R. P. Ortiz, A. Facchetti, T. J. Marks, J. Casado, M. Z. Zgierski, M. Kozaki, V. Hernandez, J. T. L. Navarrete, *Adv. Funct. Mater.* **2009**, *19*, 386; b) Y. Zhao, Y. Guo, Y. Liu, *Adv. Mater.* **2013**, *25*, 5372.

[8] a) S. Kola, J. Sinha, H. E. Katz, *J. Polym. Sci. Part B: Polym. Phys.* **2012**, *50*, 1090; b) C. Wang, H. Dong, W. Hu, Y. Liu, D. Zhu, *Chem. Rev.* **2012**, *112*, 2208.

[9] D. E. Janzen, M. W. Burand, P. C. Ewbank, T. M. Pappenfus, H. Higuchi, D. A. da Silva Filho, V. G. Young, J.-L. Brédas, K. R. Mann, *J. Am. Chem. Soc.* **2004**, *126*, 15295.

[10] J. Casado, T. M. Pappenfus, K. R. Mann, E. Ortí, P. M. Viruela, B. Milián, V. Hernández, J. T. López Navarrete, *ChemPhysChem* **2004**, *5*, 529.

[11] a) J.-L. Brédas, *J. Chem. Phys.* **1985**, *82*, 3808; b) Y.-J. Cheng, S.-H. Yang, C.-S. Hsu, *Chem. Rev.* **2009**, *109*, 5868.

[12] a) T. Takahashi, K. Matsuoka, K. Takimiya, T. Otsubo, Y. Aso, *J. Am. Chem. Soc.* **2005**, *127*, 8928; b) R. Ponce Ortiz, J. Casado, S. Rodríguez González, V. Hernández, J. T. López Navarrete, P. M. Viruela, E. Ortí, K. Takimiya, T. Otsubo, *Chem. Eur. J.* **2010**, *16*, 470.

[13] a) S. Gronowitz, B. Uppström, *Acta Chem. Scand. B* **1974**, *28*, 981; b) T. M. Pappenfus, R. J. Chesterfield, C. D. Frisbie, K. R. Mann, J. Casado, J. D. Raff, L. L. Miller, *J. Am. Chem. Soc.* **2002**, *124*, 4184; c) J. Casado, R. Ponce Ortiz, J. T. López Navarrete, *Chem. Soc. Rev.* **2012**, *41*, 5672.

[14] a) R. J. Chesterfield, C. R. Newman, T. M. Pappenfus, P. C. Ewbank, M. H. Haukaas, K. R. Mann, L. L. Miller, C. D. Frisbie, *Adv. Mater.* **2003**, *15*, 1278; b) Q. Wu, R. Li, W. Hong, H. Li, X. Gao, D. Zhu, *Chem. Mater.* **2011**, *23*, 3138.

[15] a) S. Handa, E. Miyazaki, K. Takimiya, *Chem. Commun.* **2009**, 3919; b) J.-C. Ribierre, S. Watanabe, M. Matsumoto, T. Muto, A. Nakao, T. Aoyama, *Adv. Mater.* **2010**, *22*, 4044; c) J. Li, X. Qiao, Y. Xiong, W. Hong, X. Gao, H. Li, *J. Mater. Chem. C* **2013**, *1*, 5128.

[16] J. Casado, L. L. Miller, K. R. Mann, T. M. Pappenfus, H. Higuchi, E. Ortí, B. Milián, R. Pou-Amérigo, V. Hernández, J. T. López Navarrete, *J. Am. Chem. Soc.* **2002**, *124*, 12380.

[17] S. Handa, E. Miyazaki, K. Takimiya, Y. Kunugi, *J. Am. Chem. Soc.* **2007**, *129*, 11684.
[18] T. Izumi, S. Kobashi, K. Takimiya, Y. Aso, T. Otsubo, *J. Am. Chem. Soc.* **2003**, *125*, 5286.
[19] a) Y. Suzuki, E. Miyazaki, K. Takimiya, *J. Am. Chem. Soc.* **2010**, *132*, 10453; b) Y. Suzuki, M. Shimawaki, E. Miyazaki, I. Osaka, K. Takimiya, *Chem. Mater.* **2010**, *23*, 795.
[20] G. V. Tormos, K. A. Belmore, M. P. Cava, *J. Am. Chem. Soc.* **1993**, *115*, 11512.
[21] a) M. Shahid, T. McCarthy-Ward, J. Labram, S. Rossbauer, E. B. Domingo, S. E. Watkins, N. Stingelin, T. D. Anthopoulos, M. Heeney, *Chem. Sci.* **2012**, *3*, 181; b) A. J. Kronemeijer, E. Gili, M. Shahid, J. Rivnay, A. Salleo, M. Heeney, H. Sirringhaus, *Adv. Mater.* **2012**, *24*, 1558.
[22] Y. Kunugi, K. Takimiya, Y. Toyoshima, K. Yamashita, Y. Aso, T. Otsubo, *J. Mater. Chem.* **2004**, *14*, 1367.
[23] a) M. Heeney, W. Zhang, D. J. Crouch, M. L. Chabinyc, S. Gordeyev, R. Hamilton, S. J. Higgins, I. McCulloch, P. J. Skabara, D. Sparrowe, *Chem. Commun.* **2007**, 5061; b) S. S. Zade, N. Zamoshchik, M. Bendikov, *Chem. Eur. J.* **2009**, *15*, 8613; c) A. Patra, M. Bendikov, *J. Mater. Chem.* **2010**, *20*, 422.
[24] X. Zhang, J. P. Johnson, J. W. Kampf, A. J. Matzger, *Chem. Mater.* **2006**, *18*, 3470.
[25] a) J. Cornil, D. Beljonne, J. P. Calbert, J. L. Brédas, *Adv. Mater.* **2001**, *13*, 1053; b) A. Moliton, R. C. Hiorns, *Polym. Int.* **2004**, *53*, 1397; c) A. Moliton, J.-M. Nunzi, *Polym. Int.* **2006**, *55*, 583.
[26] a) B. Lim, K.-J. Baeg, H.-G. Jeong, J. Jo, H. Kim, J.-W. Park, Y.-Y. Noh, D. Vak, J.-H. Park, J.-W. Park, *Adv. Mater.* **2009**, *21*, 2808; b) W. Hong, B. Sun, H. Aziz, W.-T. Park, Y.-Y. Noh, Y. Li, *Chem. Commun.* **2012**, *48*, 8413.
[27] a) Y. Wu, P. Liu, S. Gardner, B. S. Ong, *Chem. Mater.* **2005**, *17*, 221; b) Y. Kim, S. Cook, S. M. Tuladhar, S. A. Choulis, J. Nelson, J. R. Durrant, D. D. Bradley, M. Giles, I. McCulloch, C.-S. Ha, M. Ree, *Nat. Mater.* **2006**, *5*, 197.
[28] a) R. S. Becker, J. Seixas de Melo, A. L. Macüanita, F. Elisei, *J. Phys. Chem.* **1996**, *100*, 18683; b) G. A. Diaz-Quijada, N. Weinberg, S. Holdcroft, B. M. Pinto, *J. Phys. Chem. A* **2002**, *106*, 1266.
[29] S. Braun, W. R. Salaneck, M. Fahlman, *Adv. Mater.* **2009**, *21*, 1450.
[30] a) Y.-Y. Noh, J.-J. Kim, Y. Yoshida, K. Yase, *Adv. Mater.* **2003**, *15*, 699; b) Y.-Y. Noh, R. Azumi, M. Goto, B.-J. Jung, E. Lim, H.-K. Shim, Y. Yoshida, K. Yase, D.-Y. Kim, *Chem. Mater.* **2005**, *17*, 3861; c) S. Z. Bisri, T. Takenobu, Y. Yomogida, H. Shimotani, T. Yamao, S. Hotta, Y. Iwasa, *Adv. Funct. Mater.* **2009**, *19*, 1728; d) Y. Yomogida, T. Takenobu, H. Shimotani, K. Sawabe, S. Z. Bisri, T. Yamao, S. Hotta, Y. Iwasa, *Appl. Phys. Lett.* **2010**, *97*, 173301.
[31] Y. Qiao, J. Zhang, W. Xu, D. Zhu, *J. Mater. Chem.* **2012**, *22*, 5706.
[32] R. P. Ortiz, H. Herrera, R. Blanco, H. Huang, A. Facchetti, T. J. Marks, Y. Zheng, J. L. Segura, *J. Am. Chem. Soc.* **2010**, *132*, 8440.
[33] a) Jaguar, version 6.5 ed., Schrodinger, LLC, New York, NY, **2005**; b) B. H. Greeley, T. V. Russo, D. T. Mainz, R. A. Friesner, J.-M. Langlois, W. A. Goddard III, R. E. Donnelly Jr., M. N. Ringalda, *J. Chem. Phys.* **1994**, *101*, 4028.
[34] M. J. Frisch, G. W. Trucks, H. B. Schlegel, G. E. Scuseria, M. A. Robb, F. R. Cheeseman, G. Scalmani, V. Barone, B. Mennucci, G. A. Petersson, G. Nakatsuji, M. Caricato, X. Li, G. P. Hratchian, A. F. Izmaylov, J. Bloino, G. Zheng, J. L. Sonnenberg, M. Hada, M. Ehara, K. Toyota, R. Fukuda, J. Hasegawa, M. Ishida, T. Nakajima, Y. Honda, O. Kitao, H. Nakai, T. Vreven, J. A. Montgomery Jr., J. E. Peralta, F. Ogliaro, M. Bearpark, J. J. Heyd, E. Brothers, K. N. Kudin, V. N. Staroverov, R. Kobayashi, J. Normand, K. Raghavachari, A. Rendell, J. C. Burant, S. S. Iyengar, J. Tomasi, M. Cossi, N. Rega, N. J. Millam, M. Klene, J. E. Knox, J. B. Cross, V. Bakken, C. Adamo, J. Jaramillo, R. Gomperts, R. E. Stratmann, O. Yazyev, A. J. Austin, R. Cammi, C. Pomelli, J. W. Ochterski, R. L. Martin, K. Morokuma, V. G. Zakrzewski, G. A. Voth, P. Salvador, J. J. Dannenberg, S. Dapprich, A. D. Daniels, Ö. Farkas, J. B. Foresman, J. V. Ortiz, J. Cioslowski, D. J. Fox, in *Gaussian 09*, Revision C.01 ed., Gaussian, Wallingford, CT **2009**.